arXiv:1603.02683v1 [cond-mat.stat-mech] 8 Mar 2016

Spin slush in an extended spin ice model

Jeffrey G. Rau[1] and Michel J. P. Gingras[1,2,3]

[1]*Department of Physics and Astronomy, University of Waterloo, Ontario, N2L 3G1, Canada*
[2]*Perimeter Institute for Theoretical Physics, Waterloo, Ontario, N2L 2Y5, Canada*
[3]*Canadian Institute for Advanced Research, 180 Dundas Street West, Suite 1400, Toronto, ON, M5G 1Z8, Canada*

(Dated: March 10, 2016)

We introduce a new classical spin liquid on the pyrochlore lattice by extending spin ice with further neighbour interactions. We find that this disorder-free spin model exhibits a form of dynamical heterogeneity with extremely slow relaxation for some spins while others fluctuate quickly down to zero temperature. We thus call this state "spin slush", in analogy to the heterogeneous mixture of solid and liquid water. This behaviour is driven by the structure of the ground state manifold which extends the celebrated the two-in/two-out ice states to include branching structures built from three-in/one-out, three-out/one-in and all-in/all-out tetrahedra defects. Distinctive liquid-like patterns in the spin correlations serve as a signature of this intermediate range order. Possible applications to materials as well the effects of quantum tunneling are discussed.

The physics of glasses plays an important role in many types of physical systems; from its origins in the physics of liquids [1] further realizations have been found in disordered magnets [2], superconductors [3] and metals [4] through to soft-condensed matter [5] and even biophysics [6]. While ubiquitous, a complete understanding of glasses remains an important open problem in condensed matter physics. Connections between these vastly different contexts have proven fruitful in making progress; for example, studying conceptually and computationally simpler spin models, may inform the physics of super-cooled liquids and structural glasses [6]. However, there are complications – while spin glasses are driven by the combination of random quenched disorder and frustration, glass-forming liquids are intrinsically *disorder-free*. Finding a disorder-free spin model that realizes the diverse range of phenomena observed in glass formers, such as the dramatic slowing down of relaxation and emergence of spatially heterogeneous dynamics, is a serious challenge. Some examples of disorder-free spin models with strong freezing have been proposed [7–12]. Each of these proposals has some deficiency; be it the lack of heterogeneous dynamics, the need for multi-spin interactions, the use of uncontrolled approximations or the introduction of non-local dynamics.

In this article, we introduce a new type of cooperative paramagnet which we call *spin slush* (SS) in an extended spin ice model (ESI). This classical SS model is disorder-free and includes only first-, second- and third-neighbour Ising bilinear exchange interactions and thus lacks the pitfalls discussed above. We start from spin ice (SI), a well-studied magnetic analogue of common water ice [13], magnetic moments pointing in or out of the corner-shared tetrahedra of the pyrochlore lattice embody the proton displacements of water ice [14]. Similar to water ice, spin ice displays an extensive ground state degeneracy, and thus an associated extensive residual entropy, characterized by the two-in/two-out "ice rule" condition on each tetrahedron [13]. In SS, we find that the ground state manifold of SS is *larger* than that of SI and contains a far richer set of states. In addition to the two-in/two-out tetrahedra of the spin ice ground state manifold, there are spatially extended structures assembled from three-in/one-out, three-out/one-in and all-in/all-out tetrahedra. Built from SI defects, these structures are not simply loops or strings, but include branching tree-like features. After characterizing the static thermodynamic and magnetic properties of SS, we turn to dynamics. Approaching zero temperature, we find freezing, as in SI [15, 16], with an exponentially increasing average relaxation time. However, unlike in SI where all of the spins freeze uniformly as the temperature is lowered, the spins in the SS exhibit highly heterogeneous dynamics reminiscent of glass formers [17]. While many of the spins strongly freeze with an extremely slow relaxation rate, a fraction of the spins, organized into spatially local clusters, remain completely dynamic, relaxing almost immediately. Since this model is disorder-free, the random distribution of these dynamical spins derives solely from the overall freezing behaviour. This dynamical heterogeneity in SS at low temperatures motivates the name "spin

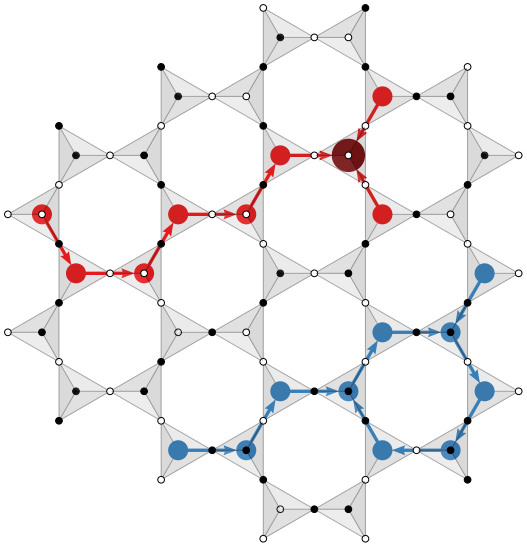

FIG. 1. **Example of spin slush ground state:** A spin slush ground state that includes all instances of the rules discussed in the main text. The colours indicate $\sigma_i = \pm 1$ (black, white) for the pyrochlore sites, and the charge Q_I for the dual lattice with $Q_I = 0$ (gray), $Q_I = \pm 1$ (red, blue) and $Q_I = \pm 2$ (dark red, dark blue). The arrow passes through the location of the minority spin for a single charge. This state contains branching lines of charge of both signs, a charge loop and a double charge tetrahedron.

slush", in analogy to "slush" where liquid water and solid ice coexist as a mixture. Finally, we speculate on the behaviour of "quantum spin slush" as well as possible experimental relevance in frustrated pyrochlore magnets.

I. MODEL

We start with a review of some results for the nearest-neighbour SI model [18] to establish our notation and motivate the SS model. The SI model is a nearest-neighbour Ising antiferromagnet on the pyrochlore lattice, $J\sum_{\langle ij\rangle}\sigma_i\sigma_j$, where $\sigma_i = \pm 1$ are the Ising spins. This can be reformulated in terms of ice rule defects, or *charges*, defined on each tetrahedron. With each tetrahedron identified with a dual diamond lattice site I, one defines the charge $Q_I \equiv \frac{1}{2}(-1)^I \sum_{i\in I}\sigma_i$, where $(-1)^I$ is a sign reflecting the sublattice of I. In this language, the nearest-neighbour SI Hamiltonian simply penalizes non-zero charges, taking the form

$$H_{\rm SI} \equiv J\sum_{\langle ij\rangle}\sigma_i\sigma_j = 8J\sum_{\diamondsuit}\left(\frac{1}{2}\sum_{i\in\diamondsuit}\sigma_i\right)^2 - NJ, \tag{1a}$$

$$= 2J\sum_I Q_I^2 - NJ. \tag{1b}$$

The ground states of this model are those with $Q_I = 0$ for all tetrahedra, i.e. the celebrated two-in/two-out states of the ice manifold. This manifold is macroscopically degenerate with a residual entropy given approximately by $S_{\rm SI} \sim (Nk_B/2)\log(3/2) \sim 0.202Nk_B$ [13]. Due to this extensive ground state degeneracy, addition of small perturbations will generically select an ordered state from this manifold at low temperatures [13].

To explore the effects of such perturbations, we consider the addition of second and third-neighbour Ising exchanges of the form

$$H \equiv J\sum_{\langle ij\rangle}\sigma_i\sigma_j + J_2\sum_{\langle\langle ij\rangle\rangle}\sigma_i\sigma_j + J_{3a}\sum_{\langle\langle\langle ij\rangle\rangle\rangle_a}\sigma_i\sigma_j. \tag{2}$$

We include only the third-neighbour exchanges that are composed of two nearest-neighbour steps. For many mechanisms that generate such interactions, for example super-exchange or through virtual crystal field excitations, one expects the interactions J_2 and J_{3a} to be generated on equal footing. The other third-neighbour exchange, J_{3b}, spanning the hexagons of the pyrochlore lattice, is only generated at higher order. Significant second- and third-neighbour exchange can be present in real materials either intrinsically [19, 20], or via partially cancellation of the leading terms [21]. One can show that for any spin ice state

$$\sum_{\langle\langle ij\rangle\rangle}\sigma_i\sigma_j + \sum_{\langle\langle\langle ij\rangle\rangle\rangle_a}\sigma_i\sigma_j = \text{const.} \tag{3}$$

We thus see that two terms are not independent and when $J_2 = J_{3a} \equiv J'$ they *cancel* each other when in the SI manifold. Moving along the $J_2 = J_{3a}$ line, the model moves away from the nearest-neighbour SI regime, but without lifting the degeneracy of the ice manifold. While SI persists as the ground state at low temperature for sufficiently small J'/J, eventually it gives way when another set of states crosses the SI manifold [22]. We thus refer to the model along this line as *extended spin ice* (ESI). It will prove useful to write this model in terms of the charges Q_I as

$$H_{\rm ESI} = 2(J-2J')\sum_I Q_I^2 - 4J'\sum_{\langle IJ\rangle}Q_IQ_J - N(J-J'). \tag{4}$$

We see that $J' > 0$ generates an attraction between nearest-neighbour charges of the *same* sign. This short-range attraction between charges will play a central role in understanding the ground and excited states of ESI.

One can show [23] that the SI manifold persists until $J' = J/4$ for $J' > 0$ and to $J' = -J/2$ for $J' < 0$ [24] The collapse of excited states when approaching $J' = J/4$ is illustrated in Fig. 2. We show only the simplest examples that cross the ice manifold, but as we shall see, there are an *infinite* set of such states. We focus on the end-point at $J' = J/4$ which we will refer to as the SS model. At this special point one can write the model as

$$H_{\rm SS} \equiv J\sum_{\langle ij\rangle}\sigma_i\sigma_j + \frac{J}{4}\sum_{\langle\langle ij\rangle\rangle}\sigma_i\sigma_j + \frac{J}{4}\sum_{\langle\langle\langle ij\rangle\rangle\rangle_a}\sigma_i\sigma_j, \tag{5a}$$

$$= \frac{J}{2}\sum_{\diamondsuit\diamondsuit}\left(\frac{1}{2}\sum_{i\in\diamondsuit\diamondsuit}\sigma_i\right)^2 - \frac{7NJ}{8}. \tag{5b}$$

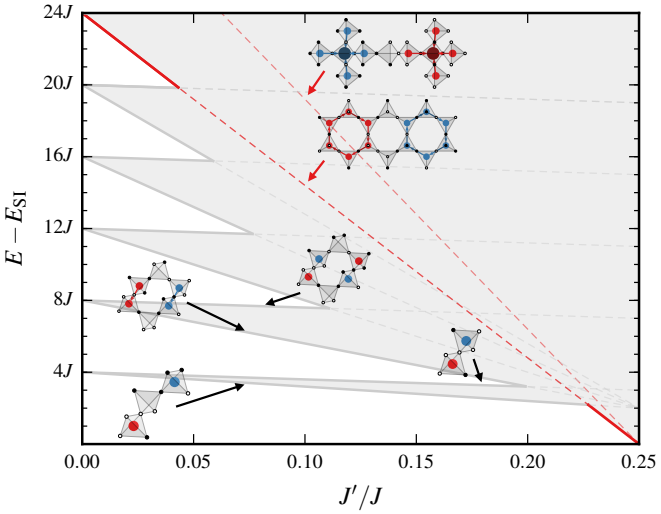

FIG. 2. **Collapse of excitations in extended spin ice:** We sketch the structure of the excited states of the model of Eq. (2) along the $J_2 = J_{3a} \equiv J'$ line. When J' is finite, the highly degenerate bands of single and double charge states are split due to the nearest-neighbour attraction embodied in the second term in Eq. (4). For the low lying bands, we illustrate the charge arrangements that are favoured and those that are disfavoured by J', using the notation of Fig. 1. Near the spin slush at $J'/J \sim 1/4$ an infinite set of excited states collapse to zero energy. We have illustrated two of the simplest examples, built from twelve charges, with energy shown by red lines.

In this form, one notes a strong similarity to the SI model of Eq. (1), except with the fundamental unit being a *pair* of tetrahedra, indicated by ⋈, rather than a single tetrahedron.

II. GROUND STATE MANIFOLD

The ground state manifold of SS is most easily characterized in terms of the variables

$$P_i \equiv \frac{1}{2} \sum_{j \in \bowtie_i} \sigma_j. \tag{6}$$

Following Eq. (5), any state with $P_i = \pm 1/2$ for all sites has the minimal energy $-3NJ/4$ and is in the ground state manifold. Alternatively, we can write this in terms of the SI charges; associating each site i of the pyrochlore lattice with a nearest-neighbour bond $\langle IJ \rangle$ of the dual diamond lattice, one has $P_i = (-1)^I (Q_I - Q_J) - \sigma_i/2$. From this expression for P_i in terms of the SI charges, it is clear that any SI state with $Q_I = 0$ for all sites also belongs to the SS manifold. In addition to the familiar SI states, many more states satisfy $P_i = \pm 1/2$. A naïve enumeration of states for an isolated pair of tetrahedra shows that beyond the 18 ice states, there are an additional 52 states, 70 total, that belong to the SS manifold [25]. These additional states include configurations with both single charge ($Q_I = \pm 1$) and double charge ($Q_I = \pm 2$) defects. The influence of the nearest-neighbour attraction of charges manifests here; pairs of like single charges can appear together, while double charges only appear with accompanying single charges of the same sign. One finds from Eq. (4) that the energy cost of having a charge can be compensated by the energy gain of having two neighbouring charges of the same sign.

From these observations, we formulate rules for constructing states that satisfy $P_i = \pm 1/2$. We formulate these rules from the perspective of specifying non-ice tetrahedra ($Q_I \neq 0$) states first, then populating the remaining tetrahedra with any compatible ice states afterward. The rules for placing the non-ice, charged tetrahedra are:

1. *Single charge rule:* The minority spin of a single charge, $Q_I = \pm 1$, must be connected to a tetrahedron carrying a single or double charge of the same sign.

2. *Double charge rule:* A double charge $Q_I = \pm 2$ must have its four nearest-neighbour tetrahedra occupied by single charges of the same sign.

3. *Neighbour rule:* A single charge, $Q_I \pm 1$, cannot have any single charges of opposite sign as nearest neighbours.

Once single and double charges have been placed such that they satisfy the above three rules, one can fill the remaining tetrahedra with *any* allowed ice rule, $Q_I = 0$, states. The first rule allows the single charge tetrahedra to form branching tree-like structures [26], where the minority spin of a given charge also belongs to the next charge in the structure. Each branch must terminate in some way compatible with the rules, so the minority spin must end up on another single charge.

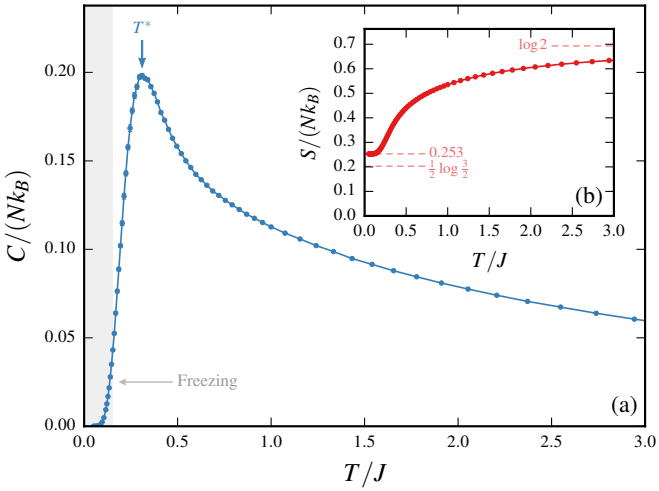

FIG. 3. **Specific heat and entropy of extended spin ice:** Finite temperature (a) specific heat, C, and (b) entropy, S, of the spin slush model for a system of 10^3 conventional cubic cells of the pyrochlore lattice. Entrance into the spin slush manifold is signaled by the peak in the specific heat at $T^* \sim 0.3J$. Residual entropy as $T \to 0$ is $S \sim 0.253Nk_B$. Freezing becomes apparent below $T \sim 0.15J$, as indicated by the shaded region.

The possibilities for terminating a branch include looping back to itself, ending on a different branch or on one of the single charges attached to a double charge. Note that these single and double charge structures must exist for both signs of the charge to satisfy the global neutrality requirement $\sum_I Q_I = 0$. The third rule implies that charge structures of opposite sign must be separated by at least one ice rule obeying tetrahedron. An illustration of an SS state incorporating all of these features, restricted to a single [111] kagomé plane, is shown in Fig. 1.

III. THERMODYNAMIC AND MAGNETIC PROPERTIES

With the ground states of SS identified, we now explore the finite temperature properties via classical Monte Carlo simulations using single-spin flip dynamics augmented with parallel tempering when appropriate. Basic thermodynamic quantities are shown in Fig. 3. The specific heat exhibits a broad peak at $T^* \sim 0.3J$, reminiscent of the peak seen in SI. This peak signals the release of entropy as one begins to enter the SS ground state manifold. This can be seen explicitly in the entropy in Fig. 3 where, below T^*, the entropy approaches the constant value $S_{\rm SS} \sim 0.253Nk_B$. As expected from the rules derived in the previous section, this is significantly *higher* than $S_{\rm SI} \sim 0.202Nk_B$ found in SI. At these low temperatures severe freezing is encountered, preventing the simulations from reaching equilibrium below $T \sim 0.15J$ [27]. The frozen states belong to the SS manifold and exhibit the single and double charge structures discussed in the previous section. We found no evidence of ordering in any of our simulations, be it conventional or via an order-by-disorder mechanism. Further, the specific heat and entropy are somewhat immune to this freezing problem, showing consistent behaviour between simulations.

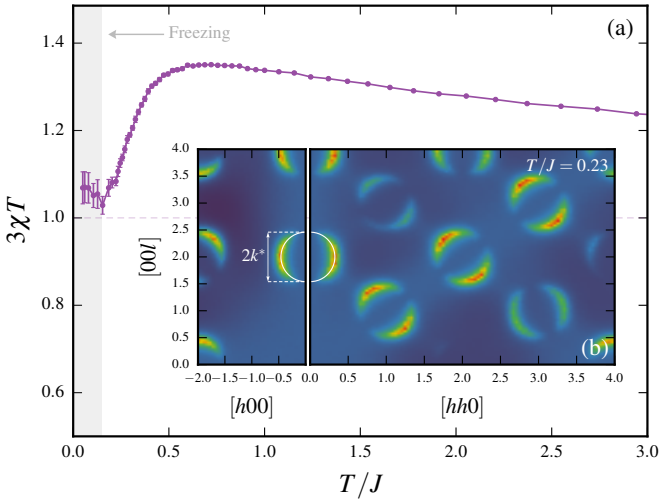

FIG. 4. **Magnetic properties of extended spin ice:** (a) Finite temperature susceptibility χ of the spin slush model for a system of 10^3 cubic cells. The susceptibility passes through maximum near $T \sim 0.6J$ before settling into a Curie-like regime with $3\chi T \sim 1$. Freezing becomes apparent below $T \sim 0.15J$, with the susceptibilities depending on the detailed spin configuration of the frozen state. (b) Transverse moment-moment correlation function $I(\mathbf{k})$ defined in Eq. (7), for the spin slush model at $T = 0.23J$ for a system of 24^3 cubic cells. Cuts in the [*hhl*] and [*h*0*l*] planes are shown. Correlations are peaked on spherical surfaces of radius $k^* \sim 0.5(2\pi/a)$ where a is the size of a cubic unit cell. These spheres are centered on the locations of the pinch-points in spin ice.

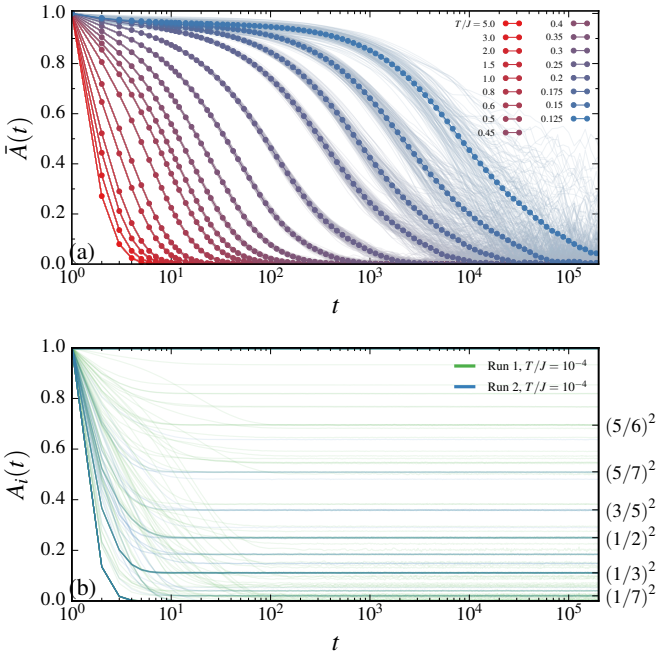

FIG. 5. **Auto-correlation functions in extended spin ice:** (a) Site-averaged auto-correlation function $\bar{A}(t)$ at various temperatures for a system of 8^3 cubic cells. As we approach low temperatures the relaxation time grows exponentially. Short-time dynamics is apparent in the initial decrease of $\bar{A}(t)$ for $t \lesssim 10^2$. The thin curves show a sample of the individual site-resolved $A_i(t)$ at each temperature, showing increasing levels of heterogeneity for $T \lesssim T^*$. (b) Site-resolved auto-correlation functions $A_i(t)$ at the very low temperature $T = 10^{-4}J$. We show two distinct annealed runs of a system of 8^3 cubic cells. Aside from essentially frozen spins with $A_i(t) = 1$, one finds many spins that relax over time scales of 10^1 or 10^2 sweeps. At long times the auto-correlation functions reach constant values $A_i(\infty)$ that are clustered about the squares of simple, rational numbers (see text).

The magnetic properties however are more sensitive.

The simplest probe of the magnetic behaviour is the uniform susceptibility, χ, shown in Fig. 4, for the moments $\boldsymbol{\mu}_i \equiv \sigma_i \hat{\mathbf{z}}_i$ pointing in/out of the tetrahedra along the local [111] direction $\hat{\mathbf{z}}_i$. At both low and high temperatures, one finds Curie-like behaviour, with $3\chi T$ constant, separated by a broad peak at $T \sim O(J)$. The constant approached as $T \to 0$ depends on the details of how the system freezes. This varies between simulations, taking on a distribution of values clustered around $3\chi T \sim 1$, reflected in the large error bars in Fig. 4. A more detailed probe of the magnetic structure can be obtained from the spin-spin correlations, as can be directly observed via neutron scattering. Recall that in SI the appearance of sharp "pinch-points" [28] in the transverse moment-moment correlation function

$$I(\mathbf{k}) \equiv \frac{1}{N} \sum_{ij} e^{i\mathbf{k}\cdot(\mathbf{r}_i - \mathbf{r}_j)} \left[\hat{\mathbf{z}}_i \cdot \hat{\mathbf{z}}_j - \left(\hat{\mathbf{z}}_i \cdot \hat{\mathbf{k}}\right)\left(\hat{\mathbf{z}}_j \cdot \hat{\mathbf{k}}\right) \right] \langle \sigma_i \sigma_j \rangle, \quad (7)$$

signals the development of long-range dipolar spin correlations. In SS, one finds sharp features in the spin-spin correlation function distinct from such pinch points. As shown in Fig. 4, below T^* the spin correlations develop into sharp rings centered on zone centers in a given plane of reciprocal space. In the full [*hkl*] space, these features lie approximately on *spheres*, reminiscent of an isotropic liquid. This analogy is even more striking in the structure factor of the spin ice charges Q_I where the intensity is approximately uniform across the sphere [23]. The wave-vector $|\mathbf{k}| \sim 0.5(2\pi/a) \equiv k^*$, where a is the size of the conventional cubic unit cell, indicates these correlations have a characteristic length of 2 cubic cells and thus represent intermediate scale correlations. These correlations are consistent with the typical size of the charged structures that appear in the ESI manifold. Indeed, as seen in Fig. 1, even the smaller of these structures can span several cubic unit cells.

These simulations confirm that the SS model does not order and the SS manifold shows all the rich charge structures at intermediate length scales implied by the SS rules. Indeed, at low temperatures a significant fraction of tetrahedra, approximately 30 – 35%, carry single-charges while a smaller but finite fraction, a percent or so, carry double charges. Similar to the susceptibility, the amount of single and double charges present at low temperatures varies somewhat from run to run, a consequence of the severe freezing problem. To better understand this issue, we now look more closely at the low temperature dynamics of SS.

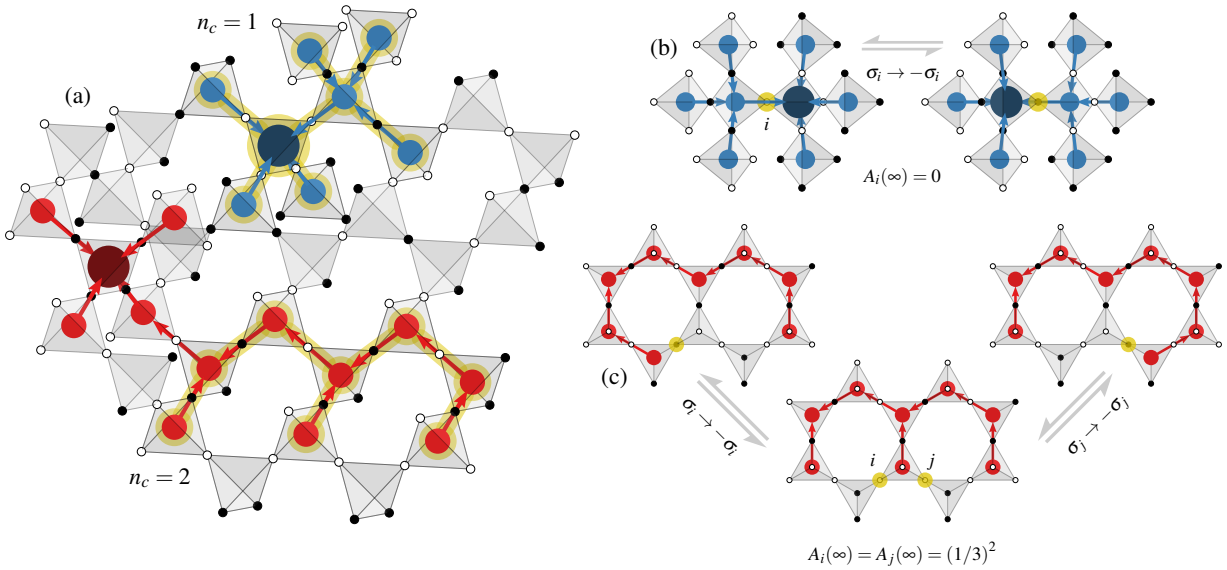

FIG. 6. **Dynamical clusters in spin slush:** We illustrate some of the dynamical clusters that can appear in the spin slush ground state manifold. In (a) we show an example of part of a state with two such clusters, one containing a single dynamical spin ($n_c = 1$) and the other containing two dynamical spins ($n_c = 2$) highlighted in gold. In (b-c) we show the accessible states of each dynamical cluster. For $n_c = 1$ the there are two states yielding an average spin of zero and thus $A_i(\infty) = 0$. For the $n_c = 2$ case, one finds three accessible states with an average spin of $\pm 1/3$ and thus $A_i(\infty) = A_j(\infty) = (1/3)^2$.

IV. DYNAMICS AND "SPIN SLUSH"

To reflect the physics of real systems with local dynamics, we employ only single spin flip, Metropolis dynamics, though we expect *any* local dynamics to give qualitatively the same behaviour. We primarily consider the site-resolved auto-correlation functions, defining $A_i(t) \equiv \langle \sigma_i(t_0)\sigma_i(t_0 + t)\rangle$, where $\sigma_i(t)$ is the Ising spin at a given Monte Carlo sweep t at site i, averaging over many initial times t_0. Generically, one would expect exponential relaxation $A_i(t) \sim e^{-t/\tau_i}$ with a characteristic relaxation time τ_i. Indeed this is found in SI, with the relaxation time being site-independent, with $\tau \sim \tau_i$ and increasing exponentially as temperature is lowered [16].

In contrast to SI, the dynamics in SS vary strongly from site to site. As temperature is lowered, most of the sites freeze, with their relaxation times becoming very long, similar to what is found in SI [15, 16]. This can be seen in the site-averaged auto-correlation function $\bar{A}(t)$ shown in Fig. 5. However, there are clear differences, namely in the initial decrease and plateau in $\bar{A}(t)$ at short times as well as in the larger site to site variance in $A_i(t)$ at low temperatures. We can understand this behaviour by looking at the $T \to 0$ limit; one finds that a fraction of sites remain highly dynamic down to very low temperatures. This is illustrated in Fig. 5, where the site-resolved auto-correlation functions are shown for $T = 10^{-4}J$. The frozen spins have $A_i(t) = 1$ at all times, while the unfrozen spins have $A_i(t)$ relaxing in 10^1 to 10^2 sweeps to a constant value $\lim_{t\to\infty} A_i(t) \equiv A_i(\infty) < 1$ [29]. A non-zero value of $A_i(\infty) < 1$ indicates that, while fluctuating, on average more time is spent in one of the states $\sigma_i = \pm 1$ than the other. For example, if σ_i is sampling uniformly from values $\sigma^{(1)}, \ldots, \sigma^{(m)}$ as a function of time, then $A_i(\infty) \sim (\frac{1}{m}\sum_{n=1}^{m} \sigma^{(n)})^2$ at long times. Fig. 5 shows that the long-time values $A_i(\infty)$ cluster about the squares of rational numbers, as would be expected from the above discussion. In these annealed simulations, the frozen spins make up the bulk of the system, while the number of unfrozen, dynamic spins is on the order of a few percent.

To better understand these dynamic spins, we examine their real space structure. We find that these spins are spatially correlated, forming clusters [30] of varying size n_c. The SS state at low temperature is thus a mixture where regions of frozen and unfrozen spins coexist. Dynamical clusters built from a small number of sites can be identified directly from the SS rules. Fig. 6 shows an SS ground state containing several of these dynamical clusters. For example, one has a single site that can be flipped while preserving all of the SS rules, representing an $n_c = 1$ dynamical cluster. A larger $n_c = 2$ cluster is also shown, where two spins can be flipped, though not independently. For both these examples we note that a large number of surrounding frozen spins are needed to construct these dynamical clusters. A naïve counting for the $n_c = 1$ case yields a fraction of unfrozen to frozen spins of $\sim 1/25 \sim 4\%$, comparable to the few percent average of unfrozen spins observed in our annealed simulations. These examples represent only a small subset of the possible dynamical clusters that can be constructed in the SS manifold. In the Supplemental information [23], we show several ways to construct dynamical clusters of *arbitrary* size as well as direct illustrations of the time evolution of dynamical clusters in simulations of small systems [23]. The presence of such dynamical clusters is not specific to the single-spin-flip dynamics used; for example, analogous dynamical clusters can be constructed for spin-exchange dynamics [23] and we expect the same holds true for *any* local dynamics.

V. DISCUSSION

Outside of any pure theoretical interest, one may be concerned with the fine-tuning required to reach the SS phase. As in SI [13], though the precise point in phase space may be difficult to reach in a material realization, the nearby regions in phase space may be controlled primarily by the SS physics. Understanding the SS manifold then allows one to understand the surrounding phases and their higher temperature properties as perturbations to the SS model. Here we discuss two types of such perturbations: deviations from the $J_2 = J_{3a}$ ESI line and quantum terms, such as transverse field or exchange.

While the effects of finite second- and third-neighbour exchange on similar models has been studied extensively [31–35], the regime along the ESI line and near the SS point remains largely unexplored. We find four neighbouring phases; the simplest are a (½,½,½) ordered phase expected from the $J_{3a} \to +\infty$ limit that appears for $J_{3a} > J/4$ and a ferromagnetic SI state expected from the $J_{3a} \to -\infty$ limit that appears for $J_{3a} < J/4$. For $J_2 < J/4$ one finds a set of layered states with sub-extensive degeneracy $\sim 2^L$ [36]. For $J_2 > J/4$ one finds a complex incommensurate ordering with wave-vector along $[h00]$ or equivalents. The SS manifold ties these phases together, *all* of which are drawn from the SS ground state manifold, with $P_i = \pm 1/2$ for all pairs of tetrahedra, and extend over large regions of parameter space. We leave the detailed investigation of these neighbouring phases and other perturbations (such as J_{3b}, dipolar interactions, etc) for future studies.

The effect of quantum non-Ising interactions on SS is potentially much richer than in SI. In the latter, the addition of transverse exchange or transverse field induces tunneling within the SI manifold yielding a $U(1)$ quantum spin liquid (QSL) [37–40]. This QSL is described by an emergent electrodynamics, complete with a gapless photon excitation [37]. However, the associated energy scale of the QSL is very small, due to tunneling only appearing at high order in perturbation theory, confining its effects very low temperatures and close proximity to the SI point [38, 41]. In the SS, quantum dynamics appear at *first order* in perturbation theory [23], and thus we expect them to be more significant than in SI. The presence of these first order matrix elements is directly reflected in the presence of single-spin-flip and spin-exchange dynamics of the SS manifold. Even with such mixing, when the perturbed Hamiltonian is projected into the SS manifold it still breaks up into infinitely many disconnected blocks, representing sets of states reachable by such local moves. The simplest blocks correspond to a small number of dynamical clusters well-separated by frozen regions. For example, there can be many $n_c = 1$ clusters as in Fig. 6, each with two states, corresponding to the freely flippable spin $|\uparrow\rangle$ and $|\downarrow\rangle$ for each cluster. Application of a transverse field $\sim -\Gamma \sum_i \sigma_i^x$ mixes the two states and gives a ground state of $(|\uparrow\rangle + |\downarrow\rangle)/\sqrt{2}$ with energy gain of $-\Gamma$ per dynamical spin. Other blocks correspond to more complicated dynamical clusters with more spatially extended structures. For example, for the large linear clusters discussed in the Supplemental information [23] the energy gain per dynamical spin is smaller, approaching $\sim -2\Gamma/n_c$ for clusters of size n_c [23]. More exotically, one can even construct states where a single dynamical cluster of size $n_c \sim O(N)$ encompasses nearly all of the spins in the system. Similar considerations apply for transverse exchange $-J_\perp \sum_{\langle ij \rangle} \left(\sigma_i^+ \sigma_j^- + \sigma_i^- \sigma_j^+\right)$. A key difference is that odd-sized dynamical clusters are guaranteed to have degenerate ground states due to Kramers' theorem. In the exchange case, the $n_c = 1$ clusters thus remain free spins and gain no energy.

We thus conclude that for quantum SS, the ground states favoured at first-order in perturbation theory will depend on the ground state energies of this zoo of clusters as well as their effective packing fractions. We leave the detailed resolution of these non-trivial questions to future work. As this model is free of the sign problem, some of these questions should be addressable through quantum Monte Carlo simulations for both a ferromagnetic transverse exchange ($J_\pm > 0$) or an arbitrary transverse field. The physics of the above dynamical clusters and the heterogeneous freezing could potentially enlighten our understanding of the phenomena of persistent spin dynamics [42]. In a more concrete setting, one may speculate that the SS could be connected to the physics observed in the QSL candidate $Tb_2Ti_2O_7$. A tantalizing clue are the short-range correlations [43] at wave-vector (½,½,½) seen in $Tb_2Ti_2O_7$ and the (½,½,½) phase obtained by perturbing SS.

In summary, we have identified "spin slush", a new cooperative paramagnet on the pyrochlore lattice found by extending spin ice with further neighbour exchanges. This classical Ising model serves as a simple example of freezing and dynamical heterogeneity in a clean, disorder-free system. The features present in the magnetic correlations and the unusual low temperature dynamics could prove useful in understanding such physics in real materials.

ACKNOWLEDGMENTS

We thank Yuan Wan for helpful comments and discussions. This work was supported by the NSERC of Canada, the Canada Research Chair program (M.G., Tier 1), the Canadian Foundation for Advanced Research and the Perimeter Institute (PI) for Theoretical Physics. Research at PI is supported by the Government of Canada through Industry Canada and by the Province of Ontario through the Ministry of Economic Development & Innovation.

Appendix A: Details of Monte Carlo simulations

For all Monte Carlo simulations we used the standard Metropolis updating scheme with single spin flip moves. For thermodynamic quantities we simulated systems of $N = 16L^3$ spins in L^3 conventional cubic unit cells of the pyrochlore lattice under periodic boundary conditions with linear size up to $L = 10$. Typically, we used $O(10^6)$ sweeps to anneal the system to each temperature and thermalize, then an additional $O(10^6)$ sweeps were used to compute observables. Error estimates were computed via the bootstrap method. For spin-spin and charge-charge correlation functions, we simulated larger systems of size up to $L = 24$, but only $O(10^5)$ sweeps were

needed to obtain accurate results. In both cases, we also used parallel tempering moves after each sweep to aid equilibriation. Longer simulations on smaller system sizes, with $O(10^7)$ to $O(10^8)$ sweeps produce results consistent with the shorter simulations on the larger systems. For dynamical quantities, a comparable number of sweeps and system sizes were used, except without the use of parallel tempering. To access the very low temperature auto-correlation function, we first slowly annealed the system to $T/J = 10^{-4}$, guaranteeing that an SS ground state was reached, then followed the same protocol as the higher temperature simulations. This was repeated many times; two of these simulations are described in the main text.

[1] L. Berthier and G. Biroli, "Theoretical perspective on the glass transition and amorphous materials," Reviews of Modern Physics **83**, 587–645 (2011).

[2] K. Binder and A. P. Young, "Spin glasses: Experimental facts, theoretical concepts, and open questions," Reviews of Modern Physics **58**, 801–976 (1986).

[3] G. Blatter, M. V. Feigel'man, V. B. Geshkenbein, A. I. Larkin, and V. M. Vinokur, "Vortices in high-temperature superconductors," Reviews of Modern Physics **66**, 1125–1388 (1994).

[4] A. Amir, Y. Oreg, and Y. Imry, "Electron glass dynamics," Annu. Rev. Condens. Matter Phys. **2**, 235–262 (2011).

[5] G. L. Hunter and E. R. Weeks, "The physics of the colloidal glass transition," Rep. Prog. Phys. **75**, 066501 (2012).

[6] T. R. Kirkpatrick and D. Thirumalai, "Colloquium : Random first order transition theory concepts in biology and physics," Reviews of Modern Physics **87**, 183–209 (2015).

[7] P. Chandra, P. Coleman, and I. Ritchey, "The anisotropic kagome antiferromagnet: A topological spin glass?" J. Phys. I France **3**, 591–610 (1993).

[8] A. Lipowski, "Glassy behaviour and semi-local invariance in Ising model with four-spin interaction," J. Phys. A: Math. Gen. **30**, 7365–7373 (1997).

[9] R. Jack, L. Berthier, and J. Garrahan, "Static and dynamic length scales in a simple glassy plaquette model," Physical Review E **72**, 016103 (2005).

[10] C. Chamon, "Quantum glassiness in strongly correlated clean systems: An example of topological overprotection," Phys. Rev. Lett. **94**, 040402 (2005).

[11] O. Cépas and B. Canals, "Heterogeneous freezing in a geometrically frustrated spin model without disorder: Spontaneous generation of two time scales," Phys. Rev. B **86**, 024434 (2012).

[12] I. Klich, S.-H. Lee, and K. Iida, "Glassiness and exotic entropy scaling induced by quantum fluctuations in a disorder-free frustrated magnet," Nature Communications **5**, 3497 (2014).

[13] S. T. Bramwell and M. J. P. Gingras, "Spin ice state in frustrated magnetic pyrochlore materials," Science **294**, 1495–1501 (2001).

[14] M.J. Harris and M.P. Zinkin, "Frustration in the pyrochlore antiferromagnets," Modern Physics Letters B **10**, 417–438 (1996).

[15] J. Snyder, J. S. Slusky, R. J. Cava, and P. Schiffer, "How 'spin ice' freezes," Nature **413**, 48–51 (2001).

[16] L. D. C. Jaubert and P. C. W. Holdsworth, "Signature of magnetic monopole and Dirac string dynamics in spin ice," Nat Phys **5**, 258–261 (2009).

[17] L. Berthier, G. Biroli, J.-P. Bouchaud, L. Cipelletti, and W. van Saarloos, *Dynamical heterogeneities in glasses, colloids, and granular media* (Oxford University Press, 2011).

[18] P. W. Anderson, "Ordering and antiferromagnetism in ferrites," Phys. Rev. **102**, 1008–1013 (1956).

[19] C. Cheng, "Long-range antiferromagnetic interactions in $ZnFe_2O_4$ and $CdFe_2O_4$: Density functional theory calculations," Phys. Rev. B **78**, 132403 (2008).

[20] A. N. Yaresko, "Electronic band structure and exchange coupling constants in ACr_2X_4 spinels (A = Zn, Cd, Hg; X = O, S, Se)," Phys. Rev. B **77**, 115106 (2008).

[21] H. R. Molavian, M. J. P. Gingras, and B. Canals, "Dynamically induced frustration as a route to a quantum spin ice state in $Tb_2Ti_2O_7$ via virtual crystal field excitations and quantum many-body effects," Phys. Rev. Lett. **98**, 157204 (2007).

[22] This line of degeneracy also exists for analogous models with N-components spins, though how the termination manifests depends on the precise value of N.

[23] See Supplemental Material.

[24] At $J' = -J/2$, the ground states include all configurations with staggered charge $Q_I = Q_0(-1)^I$. These are the ice states ($Q_0 = 0$), the single charge states ($Q_0 = 1$) and the all-in, all-out states ($Q_0 = 2$). The manifold of $Q_I = (-1)^I$ states has been discussed recently in Ref. [44], albeit starting from a very different model.

[25] We caution that a Pauling-like estimate severely underestimates the degeneracy of the SS manifold. Given that the number of tetrahedron pairs is equal to the number of sites one would estimate a residual entropy of $Nk_B(\log 2 + \log(70/2^7)) \sim 0.0896Nk_B$. This reflects that the constraints provided by $P_i = \pm 1/2$ are much less independent than in spin ice where Pauling's estimate is accurate.

[26] In the language of graph theory, the single charge structures can form directed graphs without sinks (i.e. each vertex has non-zero out degree).

[27] It is not obvious how to construct a non-local move that samples the SS manifold efficiently. Including the SI loop move does aid equilibriation, but it is only effective in regions where no single and double charge defects are present, leaving the freezing problem for future work.

[28] S. V. Isakov, K. Gregor, R. Moessner, and S. L. Sondhi, "Dipolar spin correlations in classical pyrochlore magnets," Phys. Rev. Lett. **93**, 167204 (2004).

[29] To be precise, for the long-time limit $\lim_{t\to\infty} A_i(t)$ we mean $t \gg 1$ but still much smaller than the slow timescale $\sim O(e^{J/T})$.

[30] A dynamical cluster is defined by a set of spins where $\lim_{t\to\infty} A_i(t) < 1$ and each spin is connected by a first, second or third neighbour bond to another spin in the cluster.

[31] J. N. Reimers, A. J. Berlinsky, and A.-C. Shi, "Mean-field approach to magnetic ordering in highly frustrated pyrochlores," Phys. Rev. B **43**, 865–878 (1991).

[32] T. Nakamura and D. Hirashima, "Classical antiferromagnet on the pyrochlore lattice," Journal of Magnetism and Magnetic Materials **310**, 1297–1299 (2007).

[33] G.-W. Chern, R. Moessner, and O. Tchernyshyov, "Partial order from disorder in a classical pyrochlore antiferromagnet," Phys. Rev. B **78**, 144418 (2008).

[34] P. H. Conlon and J. T. Chalker, "Absent pinch points and emergent clusters: Further neighbor interactions in the pyrochlore Heisenberg antiferromagnet," Phys. Rev. B **81**, 224413 (2010).

[35] H. Ishizuka, M. Udagawa, and Y. Motome, "Monte Carlo study of an effective Ising model for the spin-ice type Kondo lat-

tice model," in *Proceedings of the International Conference on Strongly Correlated Electron Systems (SCES2013)* (Physical Society of Japan, 2014) p. 014013.
[36] These are related to, but not identical to the layered states discussed for the J-J_2 classical Heisenberg model of Ref. [33].
[37] M. Hermele, M. P. A. Fisher, and L. Balents, "Pyrochlore photons: The U(1) spin liquid in a S=1/2 three-dimensional frustrated magnet," Phys. Rev. B **69**, 064404 (2004).
[38] A. Banerjee, S. V. Isakov, K. Damle, and Y. B. Kim, "Unusual liquid state of hard-core bosons on the pyrochlore lattice," Phys. Rev. Lett. **100**, 047208 (2008).
[39] N. Shannon, O. Sikora, F. Pollmann, K. Penc, and P. Fulde, "Quantum ice: A quantum Monte Carlo study," Phys. Rev. Lett. **108**, 067204 (2012).
[40] M. J. P. Gingras and P. A. McClarty, "Quantum spin ice: a search for gapless quantum spin liquids in pyrochlore magnets," Rep. Prog. Phys. **77**, 056501 (2014).
[41] Y. Kato and S. Onoda, "Numerical evidence of quantum melting of spin ice: Quantum-to-classical crossover," Phys. Rev. Lett. **115**, 077202 (2015).
[42] P. A. McClarty, J. N. Cosman, A. G. Del Maestro, and M. J. P. Gingras, "Calculation of the expected zero-field muon relaxation rate in the geometrically frustrated rare earth pyrochlore $Gd_2Sn_2O_7$ antiferromagnet," Journal of Physics: Condensed Matter **23**, 164216 (2011).
[43] K. Fritsch, K. A. Ross, Y. Qiu, J. R. D. Copley, T. Guidi, R. I. Bewley, H. A. Dabkowska, and B. D. Gaulin, "Antiferromagnetic spin ice correlations at (½,½,½) in the ground state of the pyrochlore magnet $Tb_2Ti_2O_7$," Phys. Rev. B **87**, 094410 (2013).
[44] L. D. C. Jaubert, "Monopole holes in a partially ordered spin liquid," SPIN **05**, 1540005 (2015).

Supplemental material for "Spin slush in an extended spin ice model"

Jeffrey G. Rau[1] and Michel J. P. Gingras[1,2,3]

[1]*Department of Physics and Astronomy, University of Waterloo, Ontario, N2L 3G1, Canada*

[2]*Perimeter Institute for Theoretical Physics, Waterloo, Ontario, N2L 2Y5, Canada*

[3]*Canadian Institute for Advanced Research, 180 Dundas Street West, Suite 1400, Toronto, ON, M5G 1Z8, Canada*

(Dated: March 8, 2016)

I. GROUND STATES ALONG EXTENDED SPIN ICE LINE

In this section we sketch a proof that the ground states for $0 \leq J' < J/4$ are the two-in/two-out spin ice manifold. Consider the decomposition of H into contributions local to each pair of tetrahedra, i.e. one writes the total energy as $H \equiv \sum_{\langle IJ \rangle} \mathscr{H}_{IJ}(\sigma)$ where

$$\mathscr{H}_{IJ}(\sigma) = \frac{J}{4}\left[\sum_{\langle ij\rangle \in I} \sigma_i \sigma_j + \sum_{\langle ij\rangle \in J} \sigma_i \sigma_j\right] + J_2 \sum_{\langle\langle ij\rangle\rangle \in \langle IJ\rangle} \sigma_i \sigma_j + J_{3a} \sum_{\langle\langle\langle ij\rangle\rangle\rangle \in \langle IJ\rangle} \sigma_i \sigma_j. \tag{S1}$$

Note that $\mathscr{H}_{IJ}(\sigma)$ depends only on the seven spins that belong to the tetrahedron pair $\langle IJ \rangle$. For a given choice of J, J_2 and J_{3a} we define the ground state energy of this seven site system as E_0^*. Now suppose we have some configuration of spins σ_i^* that has the following property: each pair of tetrahedra has minimum energy with respect to $\mathscr{H}_{IJ}(\sigma)$, that is $\mathscr{H}_{IJ}(\sigma^*) = E_0^*$ for all pairs $\langle IJ \rangle$. Informally, this states that the two tetrahedron ground states can be "tiled" across the full lattice in a consistent way. We then can infer that σ^* is a ground state of the full model H. The argument is a simple inequality; since $\mathscr{H}_{IJ}(\sigma) \geq E_0^*$ for *all* states σ by definition, we can say that

$$H = \sum_{\langle IJ \rangle} \mathscr{H}_{IJ}(\sigma) \geq \sum_{\langle IJ \rangle} E_0^* = E^*, \tag{S2}$$

where E^* is the energy of the state σ^*. Thus $H \geq E^*$ for all states σ and so σ^* is part of the ground state manifold. Enumerating the 2^7 states of the two tetrahedron system and minimizing $\mathscr{H}_{IJ}(\sigma)$, one can thus show that the $Q_I = 0$, SI states are the ground states for $0 \leq J' < J/4$.

II. SPIN AND CHARGE CORRELATIONS IN SPIN SLUSH

Here we provide further evidence of the intermediate range correlations in the SS phase at $J' = J/4$ shown in Fig. 4 of the main text. In Fig. S2 we show the charge-charge correlation function

$$S_Q(\mathbf{k}) \equiv \frac{1}{N_d} \sum_{IJ} e^{i\mathbf{k}\cdot(\mathbf{R}_I - \mathbf{R}_J)} \langle Q_I Q_J \rangle, \tag{S3}$$

where $N_d = N/2$ is the number of dual diamond lattice sites and $\mathbf{R}_I$ are the sites of the dual diamond lattice. The sharp, liquid-like features found in $I(\mathbf{k})$ are present, but with a more uniform intensity, consistent with the charges forming intermediate range structures due to the short-range attraction induces by J_2 and J_{3a}. A three-dimensional view, in the full $[hkl]$ space is shown in Fig. S3. In Fig. S2 we show the spin-spin correlation function, without the complicating effects of the transverse projection or local axes for the moments. Explicitly, we compute

$$S(\mathbf{k}) \equiv \frac{1}{N} \sum_{ij} \langle \sigma_i \sigma_j \rangle e^{i\mathbf{k}\cdot(\mathbf{r}_i - \mathbf{r}_j)}. \tag{S4}$$

The same sharp, ring-like features are seen in each scattering plane, as in the transverse moment-moment correlator shown in Fig. 4 of the main text.

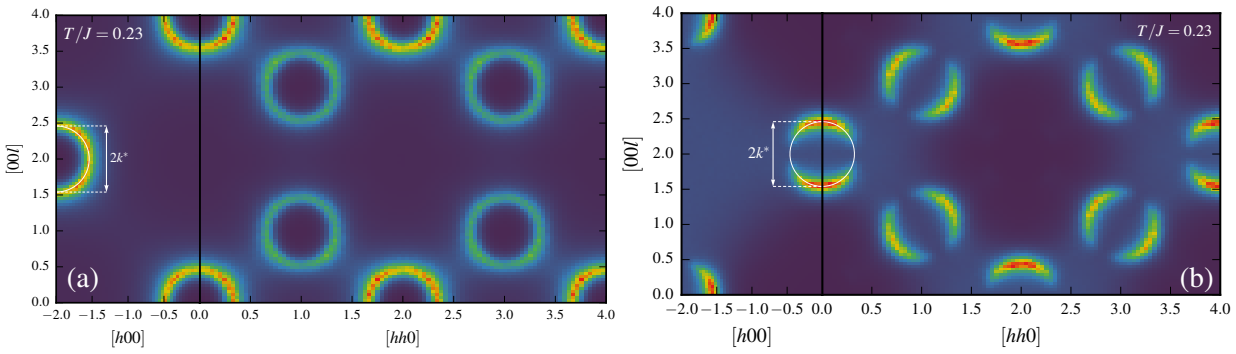

FIG. S1. **Spin and charge correlation functions in spin slush:** (a) Here we show correlation function of the spin ice charges in the spin slush state for a system of 24^3 cubic unit cells. Liquid-like correlations exist with characteristic wave-vector k^*. In contrast with the spin-spin correlation function, the intensity of the sharp features are much more uniform. (b) Here we show the spin-spin correlation function as defined in Eq. (S4) for a system of 24^3 cubic unit cells. Liquid-like correlations exist with characteristic wave-vector k^*.

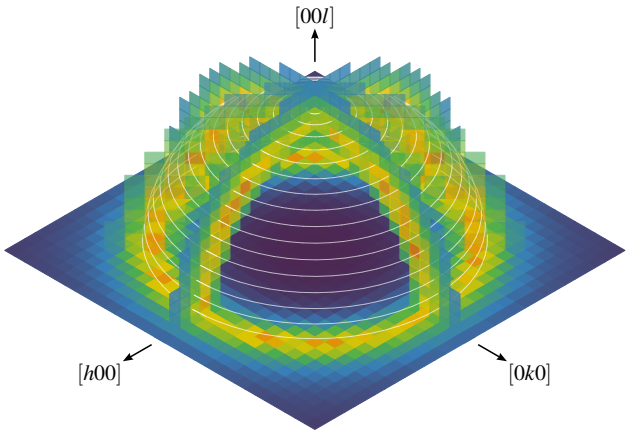

FIG. S2. **Liquid-like charge correlations in spin slush:** We illustrate the full structure of the charge-charge correlations function $S_Q(\mathbf{k})$, defined in Eq. (S3), at $T/J = 0.23$ for a system of 24^3 cubic cells. The high intensity regions approximately follow a sphere of radius $k^* \sim 0.5(2\pi/a)$ (shown by white lines) centered about zero wave-vector, reminiscent of an isotropic liquid.

III. ZOO OF DYNAMICAL CLUSTERS

We illustrate some large dynamical clusters for single-spin flip dynamics that can be constructed directly from the SS rules. First, we consider a generalization of the $n_c = 1$ cluster shown in Fig. 6 of the main text. One can easily append further single charges to the cluster to enlarge it. We show several of these larger linear clusters in Fig. S4. For each, all of the "central spins" (highlighted in gold) are dynamic, though not simultaneously. At any given point in time, only the central spins that belong to the double charge tetrahedra can be flipped. This allows the

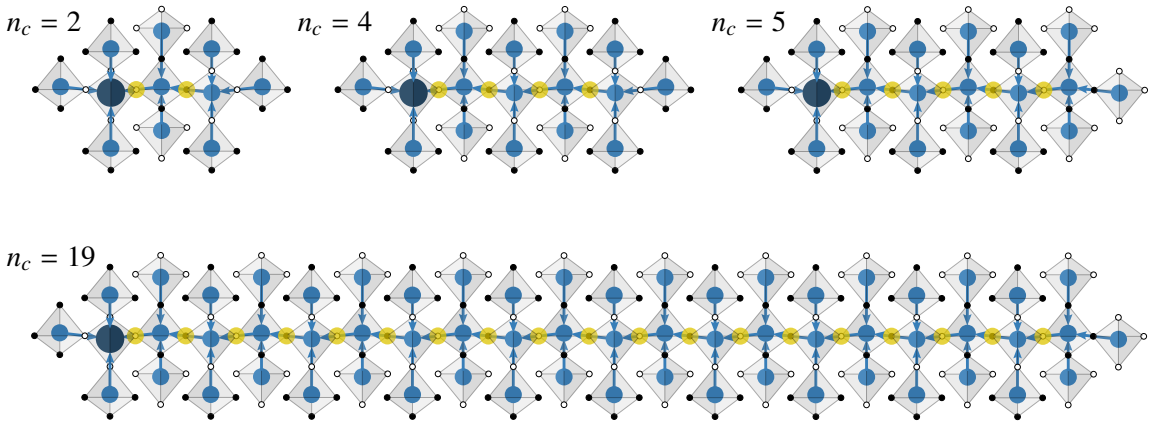

FIG. S3. **Large linear single-spin flip dynamical clusters:** We illustrate generalizations of the $n_c = 1$ dynamical cluster shown in Fig. 6 of the main text to arbitrary size n_c. By flipping neighbouring spins, the double-charge can "hop" along the length of these chains, rendering all the spins highlighted in gold dynamical.

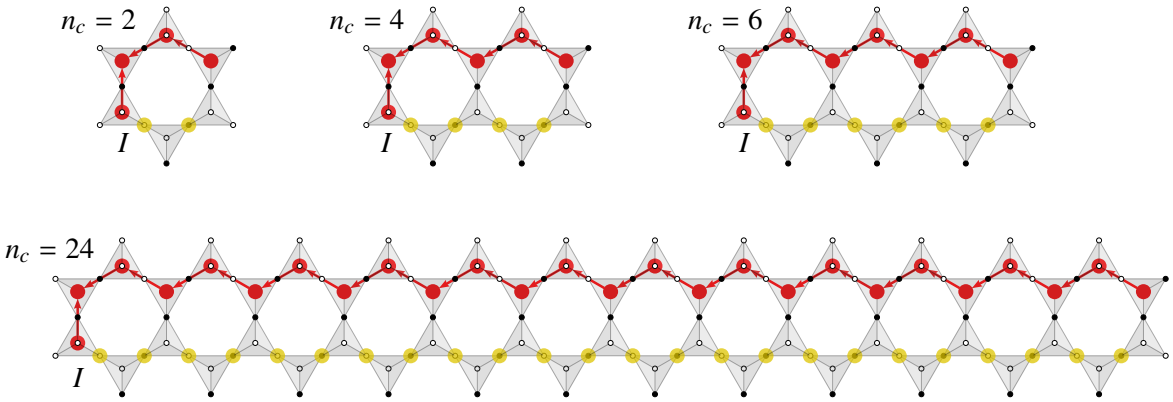

FIG. S4. **Large linear spin-exchange dynamical clusters:** We illustrate a family of dynamical clusters for spin-exchange dynamics with arbitrary size n_c. By swapping pairs of neighbouring spins, the single-charge at tetrahedron I attached to the chain can "hop" along the length of the chain, rendering all the spins highlighted in gold dynamical.

double charge to effectively "hop" randomly along the chain. We note that the topology of these clusters is flexible; the linear geometry shown here is for illustration purposes, it can be bent at any of the single charges. More complicated structures of this sort can be setup (trees, loops, etc) that allow the double charge to hop. Similar clusters can be constructed for spin-exchange dynamics, where two neighbouring spins are swapped. We illustrate one of these large clusters in Fig. S5. The "protruding" single-charge at tetrahedron I on the far left can hop along the chain by swapping neighbouring pairs of spins.

IV. EFFECT OF TRANSVERSE FIELD

To gain some understanding of the quantum effects acting within the SS manifold, we consider a simple, non-trivial cluster under the application of a transverse field at first order in perturbation theory. Similar considerations apply for transverse exchange. We start with the interaction:

$$V \equiv -\Gamma \sum_i \sigma_i^x, \tag{S5}$$

with $\Gamma > 0$. At first order we must diagonalize the interaction V projected into the SS manifold. The connection to the single-spin flip dynamics is manifest here; the non-zero matrix elements at first-order in perturbation theory correspond to those spins that can be flipped while remaining in the ground state manifold, i.e. the dynamical spins. We will ignore the rest of the lattice in this analysis, treating only this one block of the projected interaction V describing a single dynamical cluster. We take the cluster shown in Fig. S6 where there are $n_c = 3$ dynamical spins and four accessible states. We define a projection into these four states as

$$P \equiv \sum_{m=1}^{4} |m\rangle \langle m| . \tag{S6}$$

By inspection (see Fig. S6), the matrix elements within this subspace are easily found to be

$$\begin{aligned} PV|1\rangle &= -\Gamma|2\rangle, & PV|2\rangle &= -\Gamma(|1\rangle + |3\rangle), \\ PV|3\rangle &= -\Gamma(|2\rangle + |4\rangle), & PV|4\rangle &= -\Gamma|3\rangle. \end{aligned} \tag{S7}$$

More explicitly, the first-order correction to the energy in the cluster is obtained from diagonalizing the matrix

$$PVP \equiv -\Gamma \begin{pmatrix} 0 & 1 & 0 & 0 \\ 1 & 0 & 1 & 0 \\ 0 & 1 & 0 & 1 \\ 0 & 0 & 1 & 0 \end{pmatrix}. \tag{S8}$$

This can be done easily, with energy corrections

$$\delta E = \pm\Gamma\left(\frac{1-\sqrt{5}}{2}\right), \ \ \pm\Gamma\left(\frac{1+\sqrt{5}}{2}\right). \tag{S9}$$

The lowest energy configuration of this cluster corresponds to $\delta E = -\Gamma(1+\sqrt{5})/2$ with eigenvector

$$|0\rangle \propto 2(|1\rangle + |4\rangle) + (1+\sqrt{5})(|2\rangle + |3\rangle). \tag{S10}$$

More generally, for such a linear cluster of n_c spins, this is equivalent to a hopping problem on $n_c + 1$ sites with open boundary conditions. Since the non-zero off-diagonal elements are constant, the eigenvalues and eigenvectors can be found recursively. The energies are given by

$$\delta E_k = -2\Gamma \cos\left(\frac{\pi k}{n_c + 2}\right), \tag{S11}$$

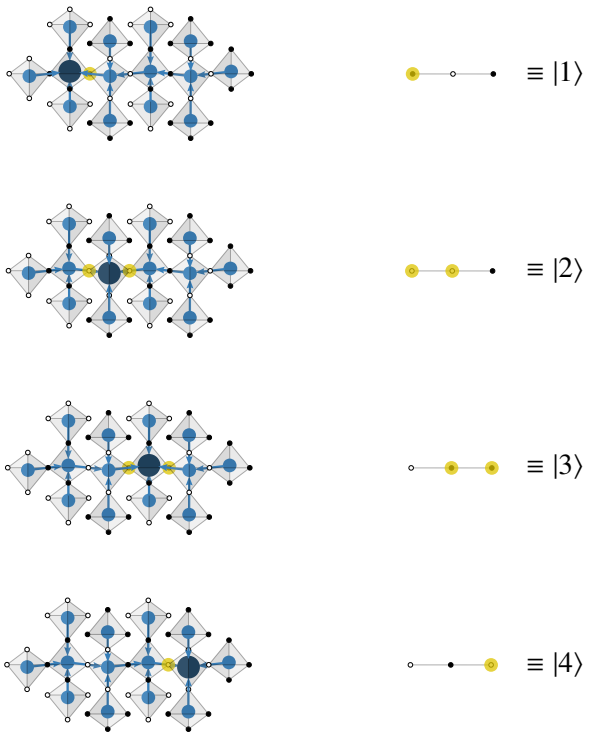

FIG. S5. **States accessible by application in a transverse field:** We show the four states of an $n_c = 3$ cluster (as in Fig. S4) that are linked by the application of a transverse field as shown in Eq. (S5). The full cluster in shown on the left, while the three relevant dynamical spins are shown on the right. The spins highlighted in gold in a given state are flippable.

for $k = 1, 2, \ldots, n_c + 1$. The ground state corresponds to $k = 1$ and takes the form

$$|0\rangle \propto \sum_{m=1}^{n_c+1} \sin\left[\frac{m\pi}{n_c+2}\right] |m\rangle \,. \tag{S12}$$

This state is delocalized across all the $n_c + 1$ states, with more weight in the states away from the end states $|1\rangle$ and $|n_c + 1\rangle$. At large $n_c \gg 1$ the energy gain due to the transverse field is thus

$$\delta E_1 = -2\Gamma \cos\left(\frac{\pi}{n_c+2}\right) \approx -2\Gamma + O(n_c^{-2}), \tag{S13}$$

or $\sim -2\Gamma/n_c$ per dynamical site, as quoted in the main text. Periodic versions of these dynamical clusters can also be constructed by connecting the ends and can be analyzed similarly.

V. DESCRIPTION OF SUPPLEMENTARY MOVIES

Illustration of dynamical spins in simulations of small systems (128 spins, 2^3 cubic cells). We show the time evolution of a state of the spin slush manifold obtained through annealing to very low temperature. At a given time the unfrozen, flippable spins are highlighted in gold. At each

time step we flip one of these unfrozen spins at random, omitting time steps where a flip of a frozen spin was rejected.

In Supplemental Movie 1, we show a highly dynamical state consisting of only single charge structures. Over the time evolution, the active, dynamical spins are distributed over many different sites of the system. In Supplemental Movie 2, we show state that contains dynamical clusters of single charges and contains a simple $n_c = 1$ double charge structure. As time evolves, the dynamics of the double-charge is activated and deactivated as the surrounding single charges fluctuate about their positions.